TECHNISCHE HOGESCHOOL DELFT

LUCHTVAART- EN RUIMTEVAARTTECHNIEK

DELFT UNIVERSITY OF TECHNOLOGY

DEPARTMENT OF AEROSPACE ENGINEERING

Memorandum M-379

Windtunnel Tests on Two Wing Segments of the ASW-19 Sailplane

by

L.M.M. Boermans
H.J.W. Selen
M.L. Wijnheijmer

Delft - The Netherlands

August 1980.

1. Introduction

At the Delft University of Technology an investigation was conducted to determine the low-speed two-dimensional aerodynamic characteristics of the Wortmann FX-61-163 airfoil as manufactured on the inner wing of the fiberglass Standard Class sailplane ASW-19 by Alexander Schleicher Segelflugzeugbau, Poppenhausen.
Also investigated were the characteristics of a part of the outer wing, where the airfoils are formed by linear lofting between FX-61-163 and FX-60-126 at the tip and a linear lofted geometric washout of 2 degrees.
The windtunnel models were parts of the inner and outer ASW-19 wing, granted by Schleicher. This offered the opportunity to compare the actual airfoils achieved in serial production with the design airfoils and to compare windtunnel test results and calculated characteristics.
In addition measurements were made with "Johnson's simulated bug pattern" on the inner wing section.

2. Model description

The windtunnel models 1 and 2 are situated in the ASW-19 wing as shown in figure 1. From the root up to 59% semispan the wing is untwisted and has the airfoil FX-61-163. From 59% semispan up to the tip the wing is linear lofted from FX-61-163 to FX-60-126, while a linear lofted washout of 2 degrees is applied.

Model 1 was obtained from a wing used for static strength tests and model 2 was built in the mould for the present windtunnel tests. The surfaces of both models are corresponding to normal serial production wings.

Model 1 was tested first to study the flow behaviour and to determine the lift-drag characteristics, where the lift was derived from wall pressure measurements. For subsequent accurate lift and pressure distribution measurements the model was provided with 107 pressure orifices (nominal diameter 0,4 mm) situated in the middle of the modelspan.

The wing section coordinates and the location of the pressure orifices were measured very accurately. As shown in figure 2 the actual airfoil is thicker than the design airfoil FX-61-163.

Model 2 has a fixed wing section (no aileron). In figure 3 the design airfoils FX-61-163 and FX-60-126 are plotted together with the design model mid-span section named FX-163-126. Figure 4 shows for the model midspan the design shape and the measured actual airfoil shape; again the actual shape is thicker than the design shape. Model 2 was tested only without pressure orifices (flow behaviour, drag characteristics); because the results differ only slightly from model 1 results, it was decided not to provide model 2 with pressure orifices.

3. Windtunnel and test equipment

The windtunnel used is the low-speed low-turbulence windtunnel of the Department of Aerospace Engineering at Delft University of Technology. The tunnel is of the closed return type and has an interchangeable octagonal test section of 1.80 m wide and 1.25 m high (figure 5). The turbulence level in the test section varies from 0.018% at 10 m/s to 0.043% at 60 m/s.
Attachment of the models takes place by rectangular end-plates which are flush with the turntables in the upper and lower tunnel wall. The axis of rotation is parallel to the model quarter chord line and crosses the middle of the model mid-span chord.

Wall pressures were measured at 15 stations (equally spaced at 50 mm) in the plane of the mid-span section on each tunnel side wall. The position of these stations was symmetrical with respect to the quarter chord point of the model mid-span section.

A wake survey rake, mounted on a cross beam, was positioned with the tips of the total pressure tubes approximately a quarter chord length of the mid-span section downstream the model. The wake rake employed 17 total pressure tubes equally spaced at 5 mm and 6 static pressure tubes. A pitot-static tube was mounted in the plane of the mid-span section on the tunnel wall opposite the lower surface of the model.

All pressures were obtained by using an automatic reading multi-tube liquid manometer (200 tubes).

The behaviour of the airflow was investigated by means of an oilfilm technique and a stethoscope. Model 2 was investigated with tufts too.

4. Tests

Model 1 has been tested twice. In the first period, when the model was not equiped with pressure orifices, the flow behaviour was investigated and drag was measured with the wake rake placed behind the model midspan. A provisional lift coefficient was derived from wall pressure measurements. In addition, measurements with "Johnson's simulated bug pattern" (see picture of fig. 5) were executed.
In the second period pressure distributions were determined and drag was measured again with the wake rake placed 0.15 m below the plane of the midspan section (i.e. the row of pressure orifices).
The measured Reynolds number range was from $1x10^6$ up to $3x10^6$.
Investigations were done at angles of attack between -6 and 20 degrees.
Model 2 tests were similar to model 1 first period tests (without bug pattern). Here the investigated Reynolds number range was from $0.85x10^6$ to $2x10^6$.

5. Data reduction

When using large models, tunnel wall interference is not negligible. As an indicative example fig. 6 shows calculated potential flow pressure distributions for the actual inner wing airfoil (model 1) with and without tunnel wall interference effects, i.e. lift interference and blockage due to airfoil thickness. The pressure distributions are calculated by the panel method of ref. 1 in which both the airfoil contour and the walls are covered with vortex panels. Of course, viscous effects due to the presence of the boundary layer and the effect of the curvature of the wake (which appeared to be important at this airfoil), nor blockage due to the wake are taken into account.

For determining the free flight characteristics from the windtunnel measurements the well-known correction method of Allen and Vincenti, ref. 2, was applied. Therefore, static pressure measurements were reduced to standard pressure coefficients by using the apparent dynamic pressure (i.e. that appropriate to the model position in the empty tunnel) as reference. By numerically integration the section normal force coefficients and pitching-moment coefficients about the quarter-chord were obtained. Section profile-drag coefficients were computed from the wake rake total and static pressures using Pfenninger's method (ref. 3). The lift coefficient was determined using the relation

$$c_\ell = \frac{c_n}{\cos\alpha} - c_d \tan\alpha$$

Finally, corrections were applied to the coefficients and angle of attack according to the relations (94) given by Allen and Vincenti.

In the standard data reduction program procedures are included to calculate the pressure distribution on the nose of the airfoil (to catch any pressure peakes which might develop there) and at the trailing edge, because the number of pressure orifices in these regions is often limited. The calculated pressures are denoted by an asterisk in the plots, the measured pressures are denoted by a triangle.

6. Results

Model 1:

The lift, drag and pitching-moment coefficients are presented in fig. 7.

Excessive forces restricted the measurements to $\alpha = 6^{o}$ at Re = $3x10^{6}$. Fig. 8 shows the position of transition at the Reynolds number $2x10^{6}$ as determined by a stethoscope, from pressure distributions and from oil flow patterns.

A selection of pressure distributions for Re = $1.5x10^{6}$ is presented in figure 9.0 up to figure 9.11.

It is noted that the pressure distribution and angles of attack in fig. 8 and 9 are not corrected according to Allen and Vincenti.

On the lower surface a laminar separation bubble is clearly indicated in the pressure plots at all Reynolds numbers and angles of attack above approximately -3^{o}. At the lower end of the low-drag bucket, when transition moves rapidly in forward direction at decreasing angle of attack, no bubbles were found on the lower surface. On the upper surface the bubble is present at angles of attack up to approximately 6^{o}. At higher angles of attack transition becomes the "normal" instability type (no bubble); it should be noted that also in these cases transition is indicated by a hump in the pressure distribution (see $\alpha = 8^{o}$), caused by the change of boundary layer displacement thickness and hence effective airfoil contour.

Maximum lift is at $\alpha = 10^{o}$. At higher angles of attack turbulent separation moves forward rapidly as indicated in the pressure plots. Nevertheless, the pressure distribution developes such as to cause a gradual stall.

The slight tapering of the model did not influence the flow behaviour.

Fig. 10 shows a comparison of calculated results for the design airfoil, the actual airfoil, present measurements and results presented in the Stuttgarter Profilkatalog I, ref. 4. The discrepancy between calculated and measured lift versus angle of attack curve is mainly due to the curvature of the wake which acts as a fluid flap; this effect will be incorporated in the next version of the computer program. This version will also include the possibility to calculate the effect of turbulence (and sound) on the characteristics.

The sharp increase in calculated drag for the actual airfoil at c_1 = 0.1 and the wavy character of the drag curve is due to the sensitiveness of the present calculation procedure for chord-wise velocity gradients. In general the calculated drag is lower than the measured drag.

Model 2:

This model was tested at about the same airspeeds as model 1, resulting in somewhat lower Reynolds numbers due to smaller model mean chord. Stethoscope measurements, oil flow patterns, tuft studies and measurements of spanwise drag distribution showed that the tapering of the model was of minor influence regarding the flow behaviour when turbulent separation occurs behind 95% local chord.
The location of transition at Re = 1.25×10^6, measured by a stethoscope, is given in figure 11.
Oil flow patterns, made at practical situations, showed at Re = 0.85×10^6 a laminar separation bubble on the upper surface at $\alpha = 5^\circ$ and on the lower surface at $\alpha = 8^\circ$, whereas at $\alpha = 8^\circ$ there is no bubble on the upper surface. At Re = 1.25×10^6 and $\alpha = 0^\circ$ the bubble is found on both sides of the airfoil. No bubble could be detected on both sides of the airfoil at $\alpha = -2^\circ$ and Re = 2.0×10^6. Some flow pictures are presented in fig. 12. The model was not provided with pressure orifices because the drag coefficient, in this case non-dimensionalized by the measured mean wall velocity, only slightly deviated from model 1 measurements, as shown in fig. 13. In fig. 14 drag coefficients for alle investigated Reynolds numbers are shown.

7. Simulated bug pattern measurements

From gliding practice the serious degradation of performance caused by insects collected on the leading edge of the wing, or by collection of rain, is well known.

In the United States performance of gliders are measured with an "artificial bug pattern", consisting of rows of little squares of silver duct tape on the leading edge of the wing, thus hoping to simulate a fairly severe collection of insects (ref. 5).

Johnson's bug pattern was duplicated here as shown in figure 5. At three practical flow conditions the drag distribution along 0.40 m span was measured. The results in fig. 15 show that the drag occasionally depends very much on the spanwise position, i.e. bug pattern. A fixed high and low drag position was chosen in order to determine the mean drag coefficient as presented in figure 16; the lift coefficient was found from the wall pressures and the correlation between wall pressures and lift coefficient of the clean wing. The figure presents the characteristics for $Re = 1.5 \times 10^6$ and for some practical angle of attack/Reynolds number combinations, both for the clean and the buggy wing. As expected the insect impact simulation appreciably increases the drag: in consequence the speed polar will considerably deteriorate.

8. References

1. Gooden, J.H.M. A numerical method of calculating two-dimensional wind tunnel wall interference on multi-element airfoils in incompressible, inviscid flow. Report to be published Delft University of Technology, 1978.

2. Allen H.J. and Vincenti, W.G. Wall interference in a two-dimensional-flow wind tunnel, with consideration of the effect of compressibility. NACA Report no.782. 1944.

3. Pfenninger, W. Vergleich der Impulsmethode mit der Wägung bei Profilwiderstandsmessungen, Mitteilung 8 der ETH, Zürich, 1973.

4. Althaus, D. Stuttgarter Profilkatalog I. Institut für Aero- und Gasdynamik der Universität Stuttgart, 1972.

5. Johnson, R. A flight test evaluation of the ASW-19 Soaring, August 1977.

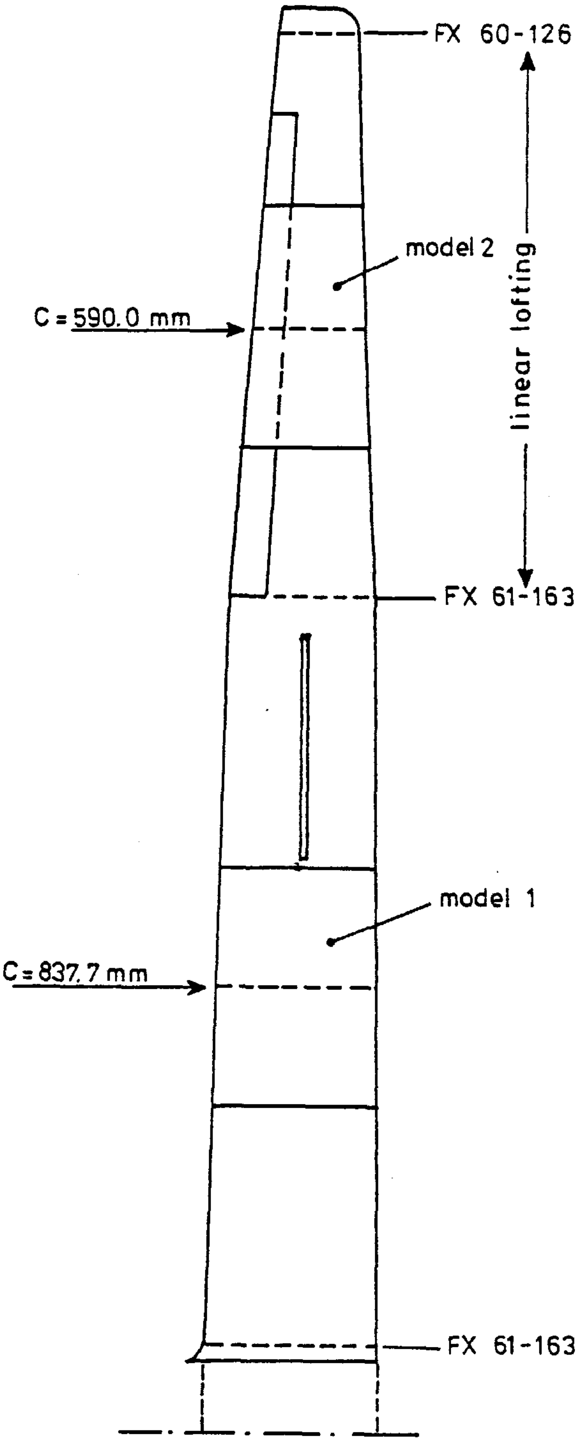

Fig. 1. Position of the models in the ASW-19 wing.

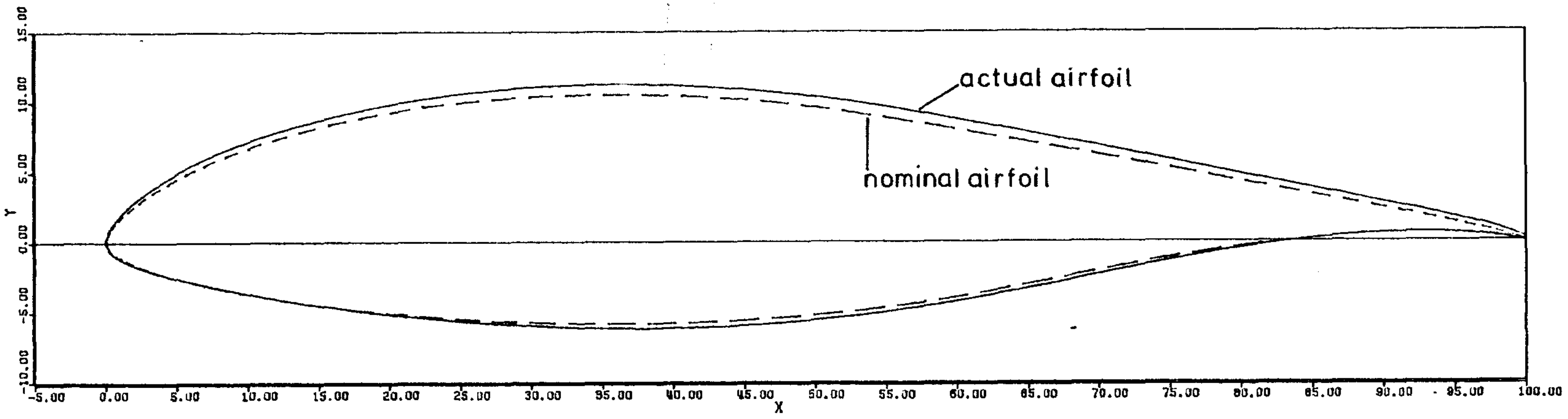

Fig. 2. Actual and nominal airfoil sections FX61-163.

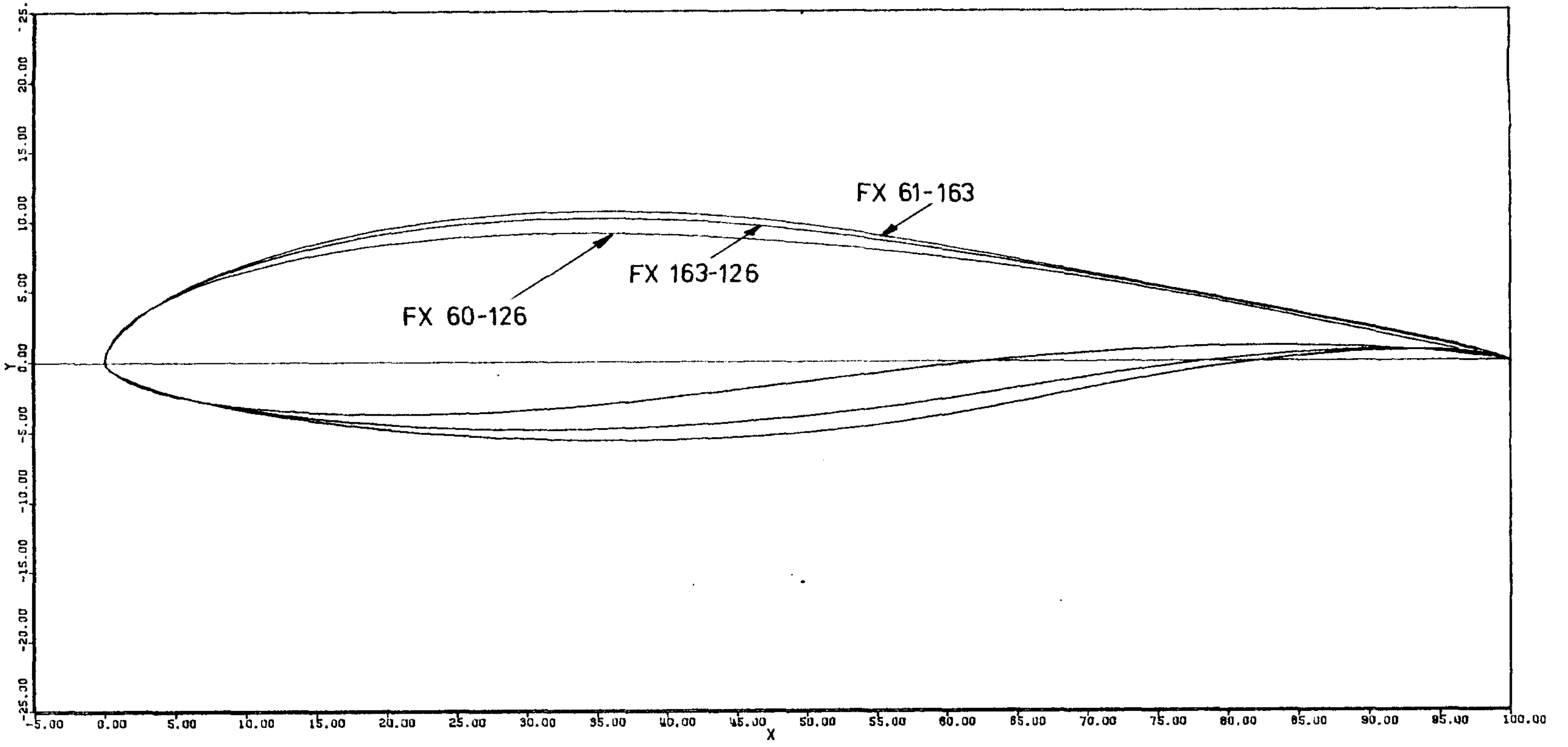

Fig. 3. Comparison of the design airfoils of the outer wing: FX 61-163
FX 163-126 (design model mid-span section)
FX 60-126.

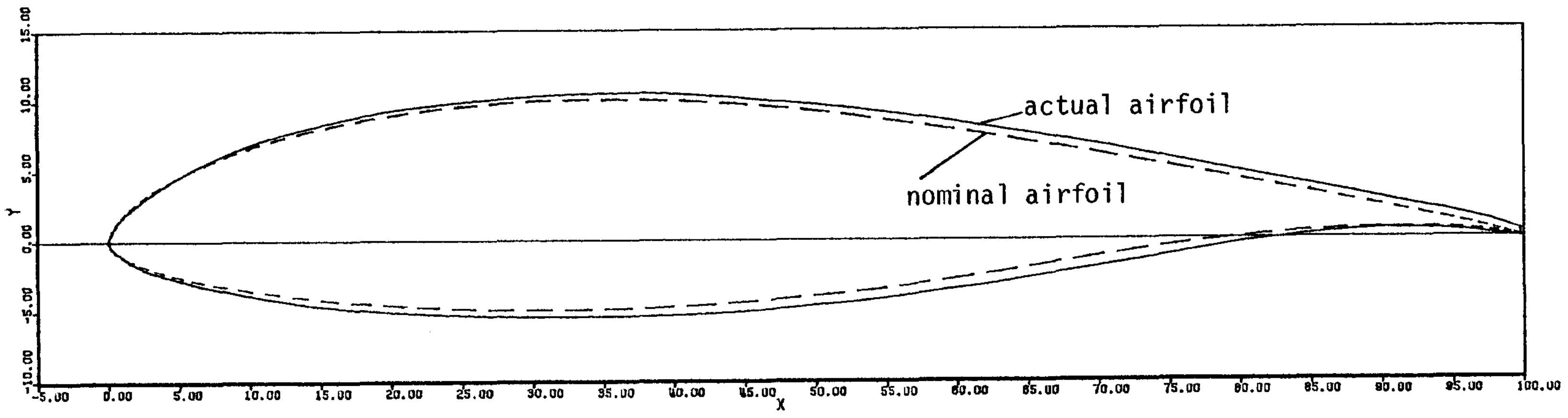

Fig. 4. Actual and nominal airfoil sections FX163-126.

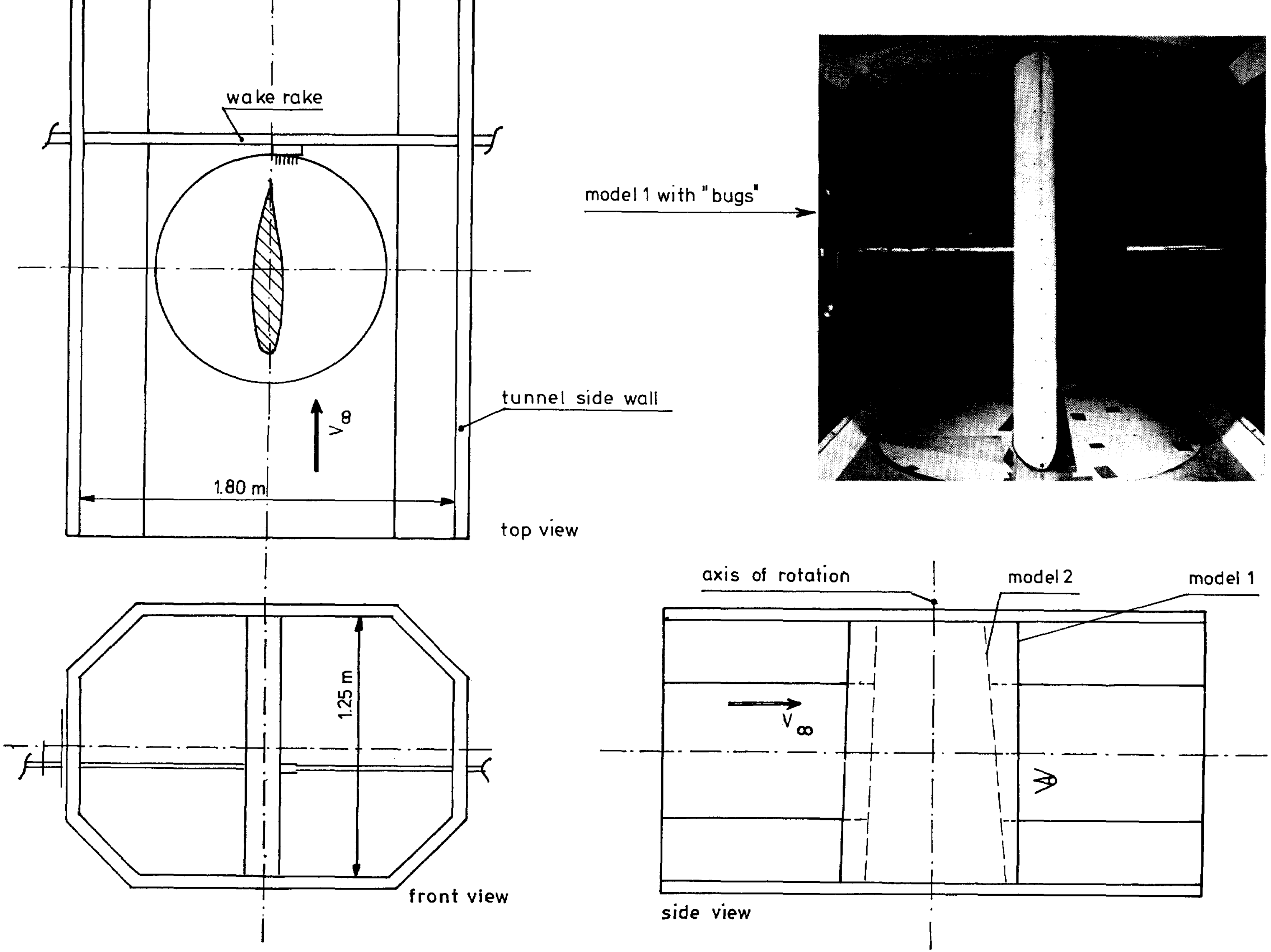

Fig. 5. Test set-up.

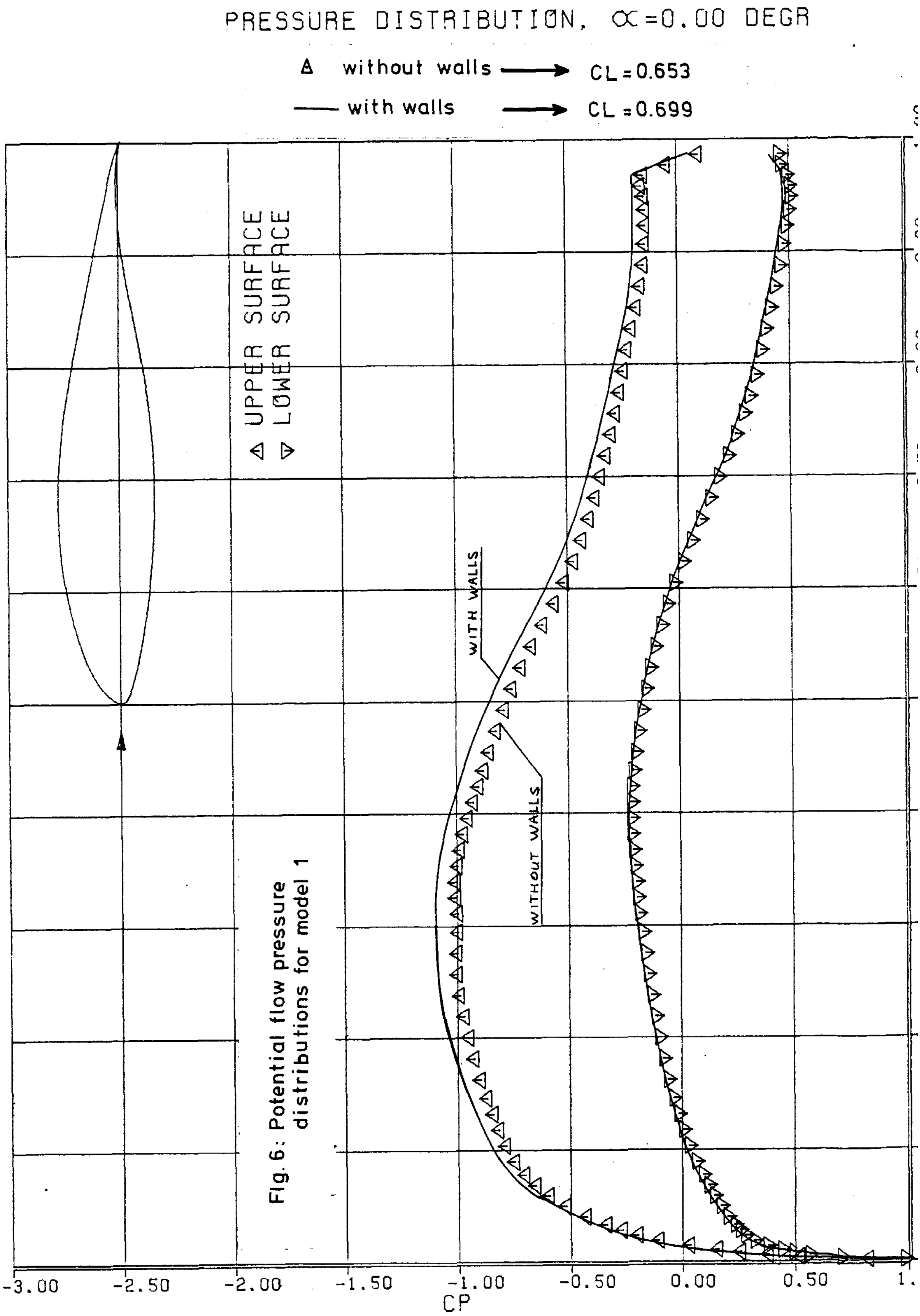

Fig. 6: Potential flow pressure distributions for model 1

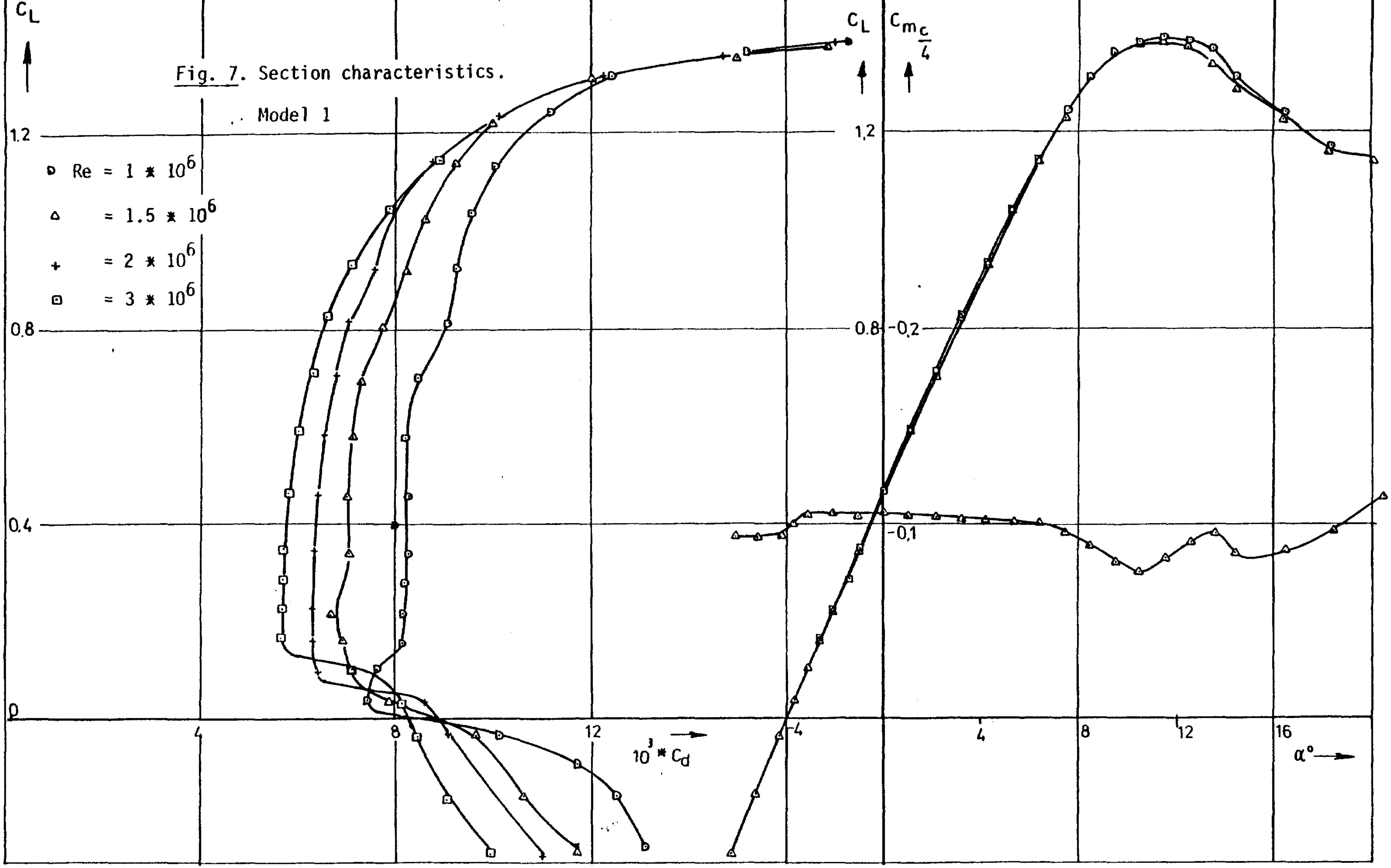
Fig. 7. Section characteristics.

Model 1

Fig. 8. Results of flow investigation on model 1.

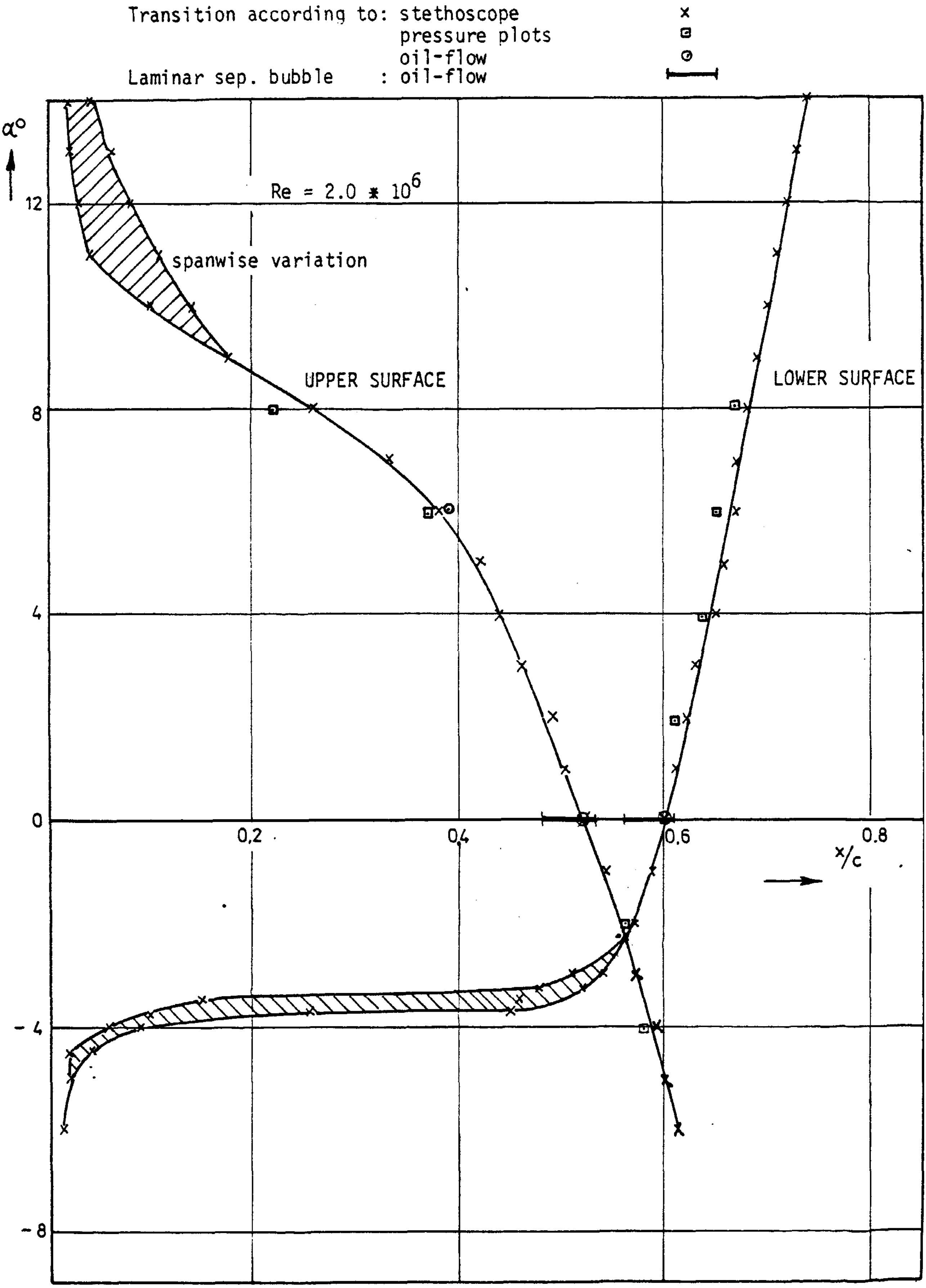

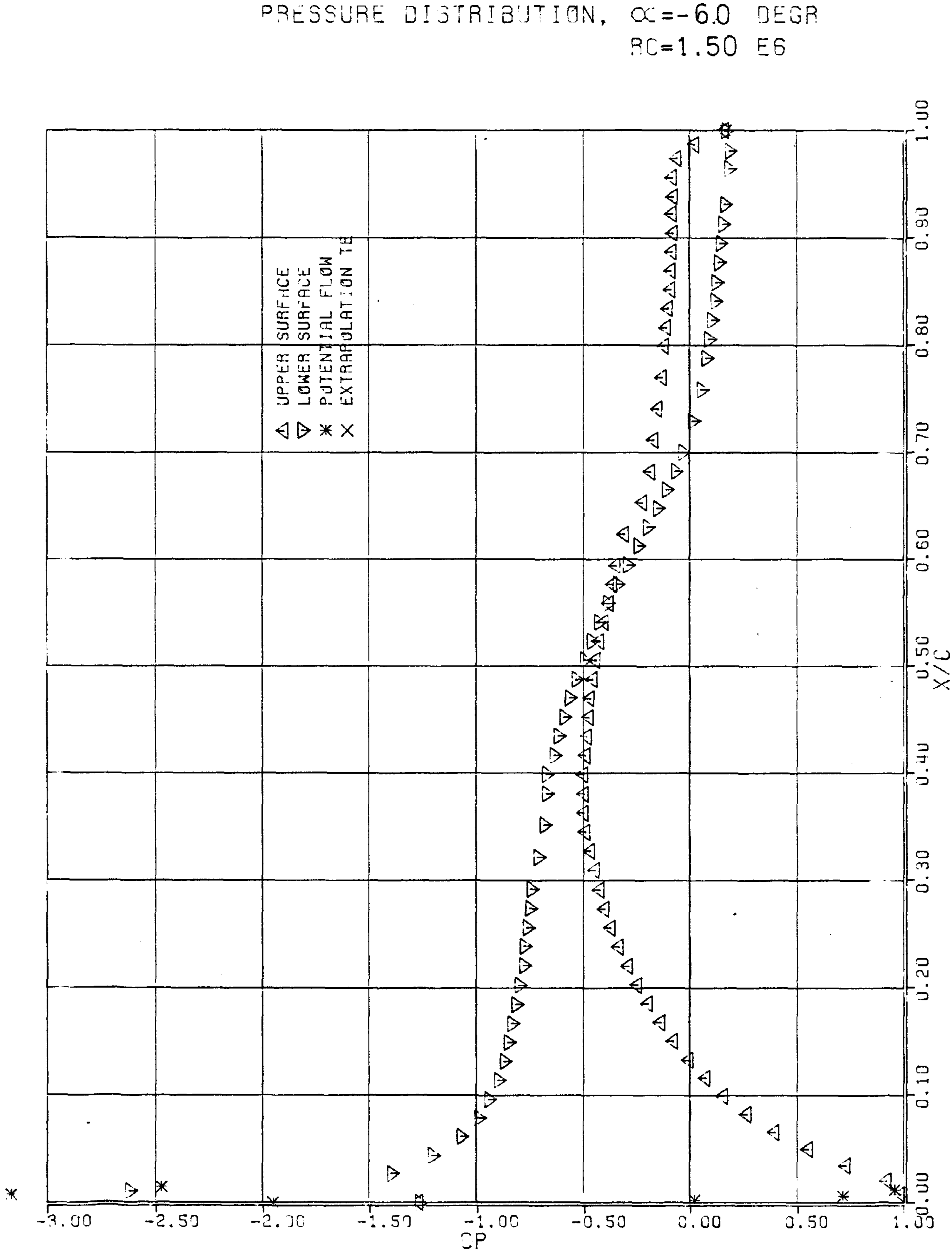

Figure 9.0 : Measured pressure distribution, model 1

PRESSURE DISTRIBUTION, α=-4.0 DEGR
RC=1.50 E6

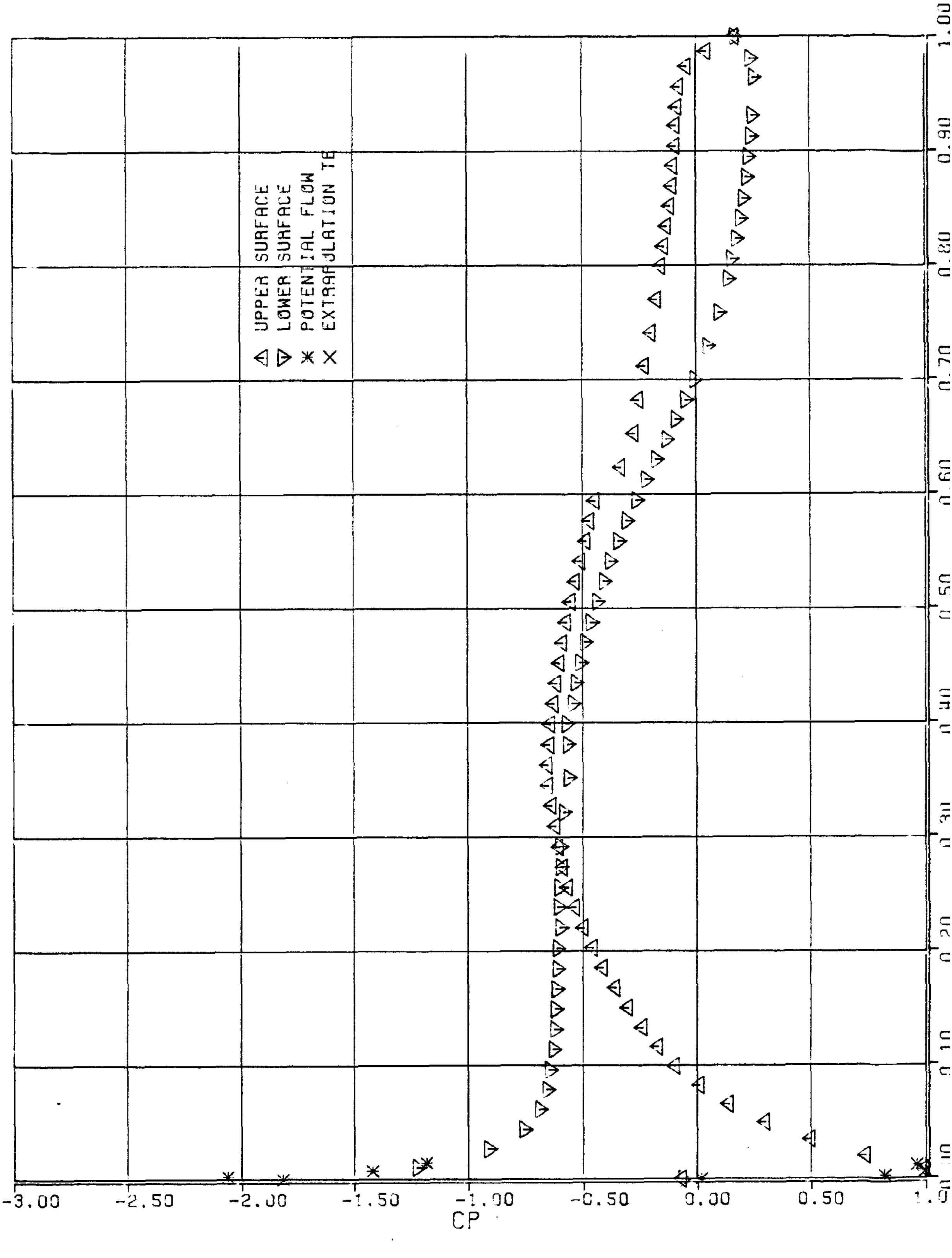

PRESSURE DISTRIBUTION, α=-2.0 DEGR
RC=1.50 E6

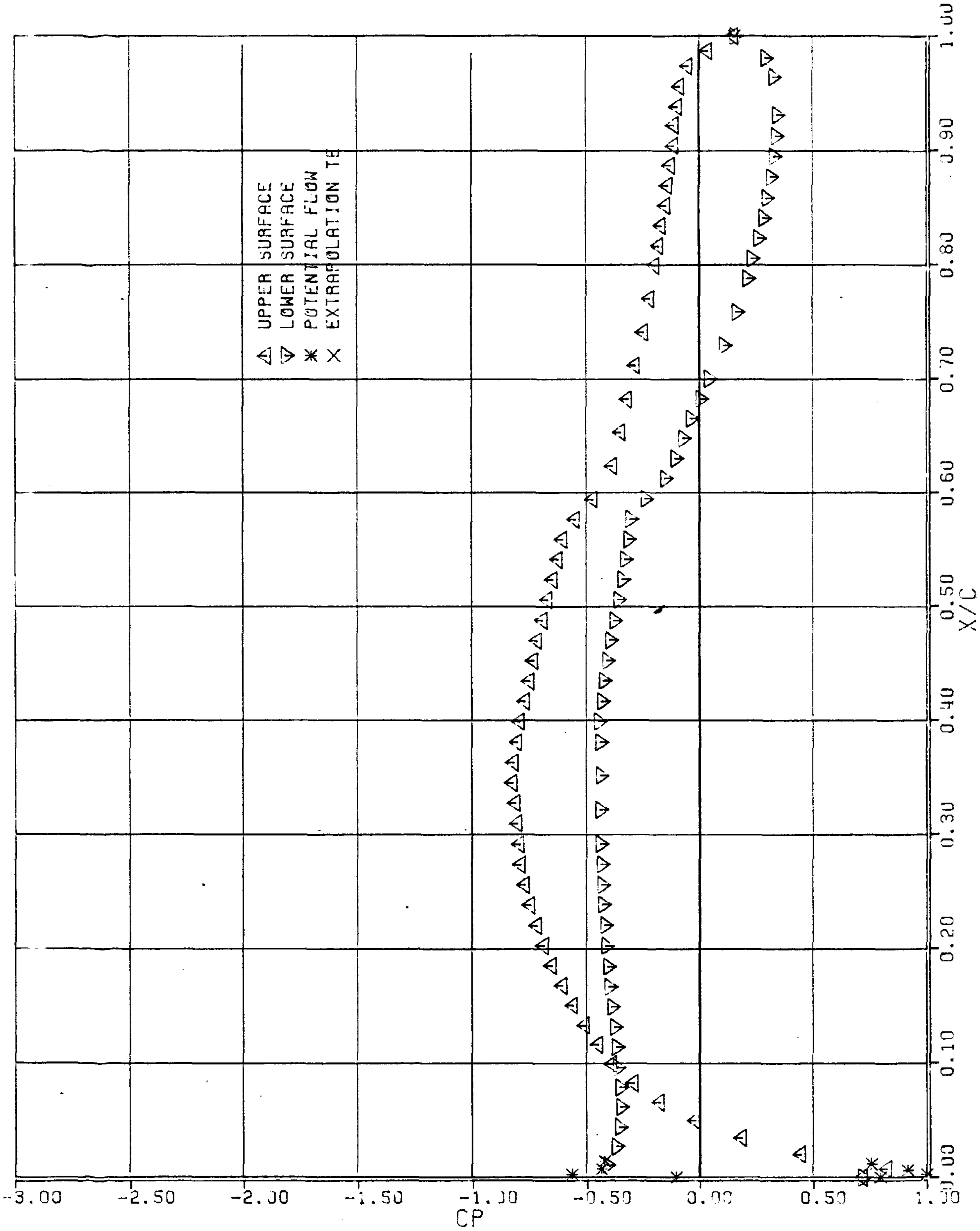

Figure 9.2 Continued

PRESSURE DISTRIBUTION, α=0.0 DEGR
RC=1.50 E6

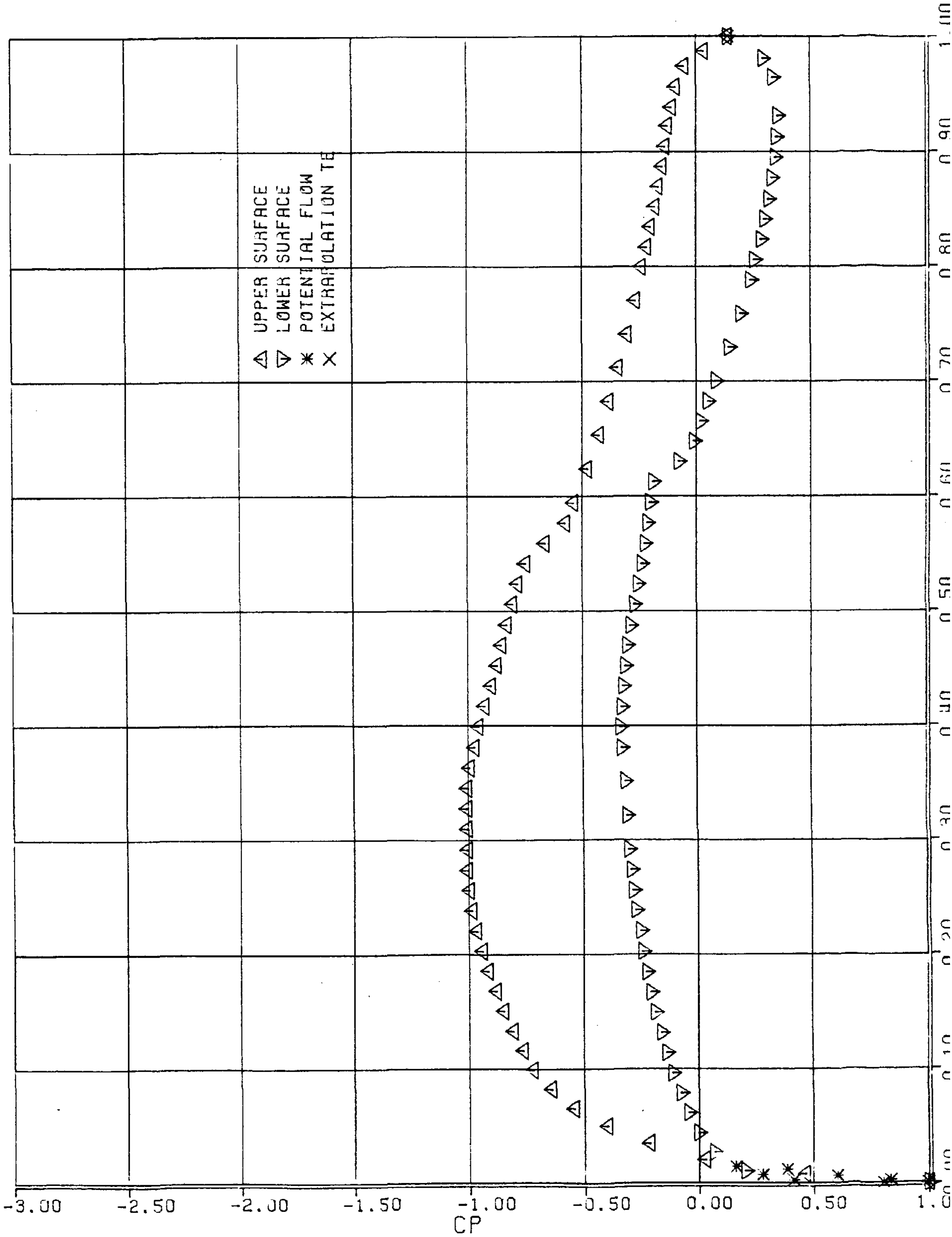

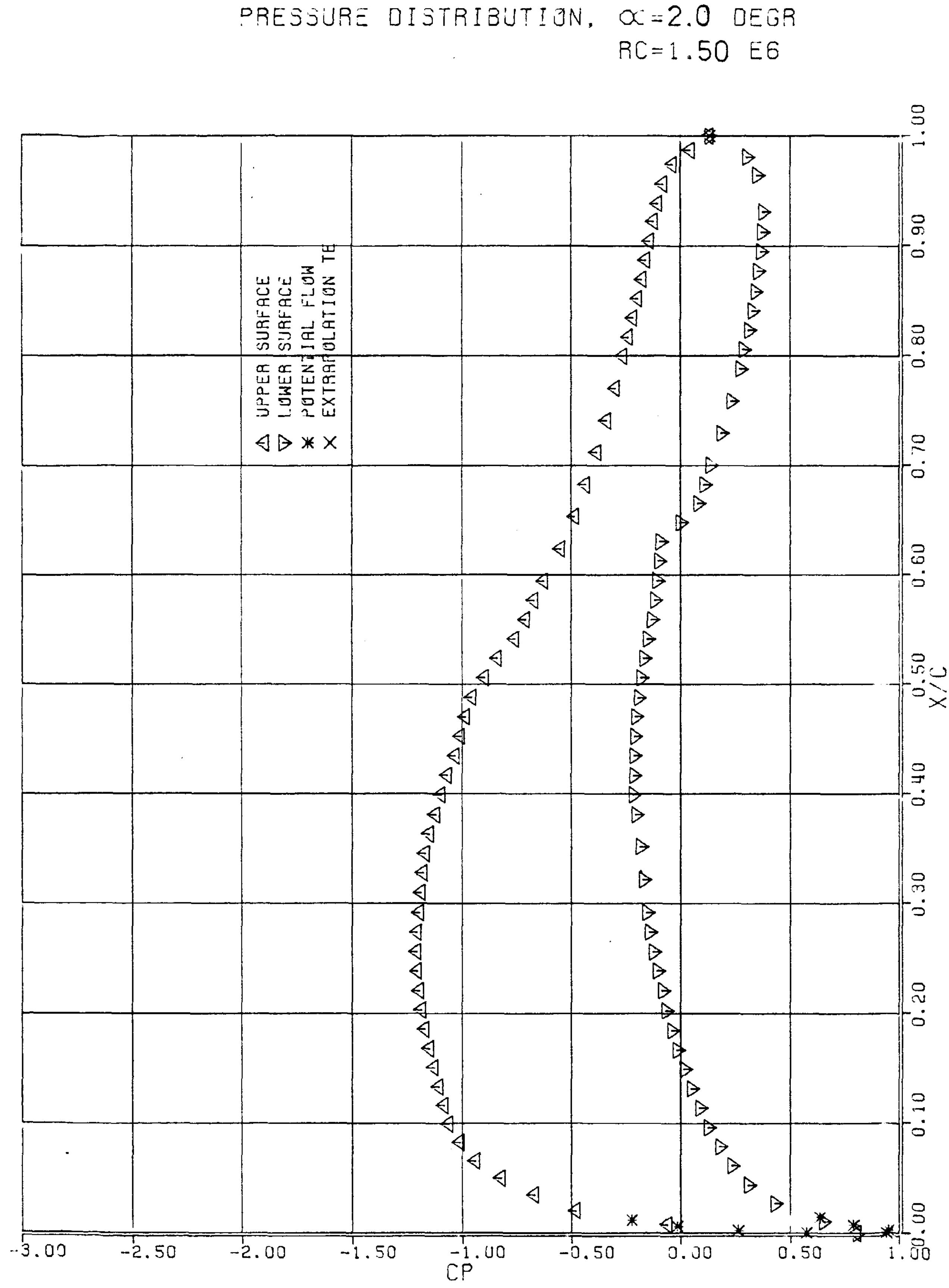

Figure 9.4 : Continued

PRESSURE DISTRIBUTION, α=4.0 DEGR
RC=1.50 E6

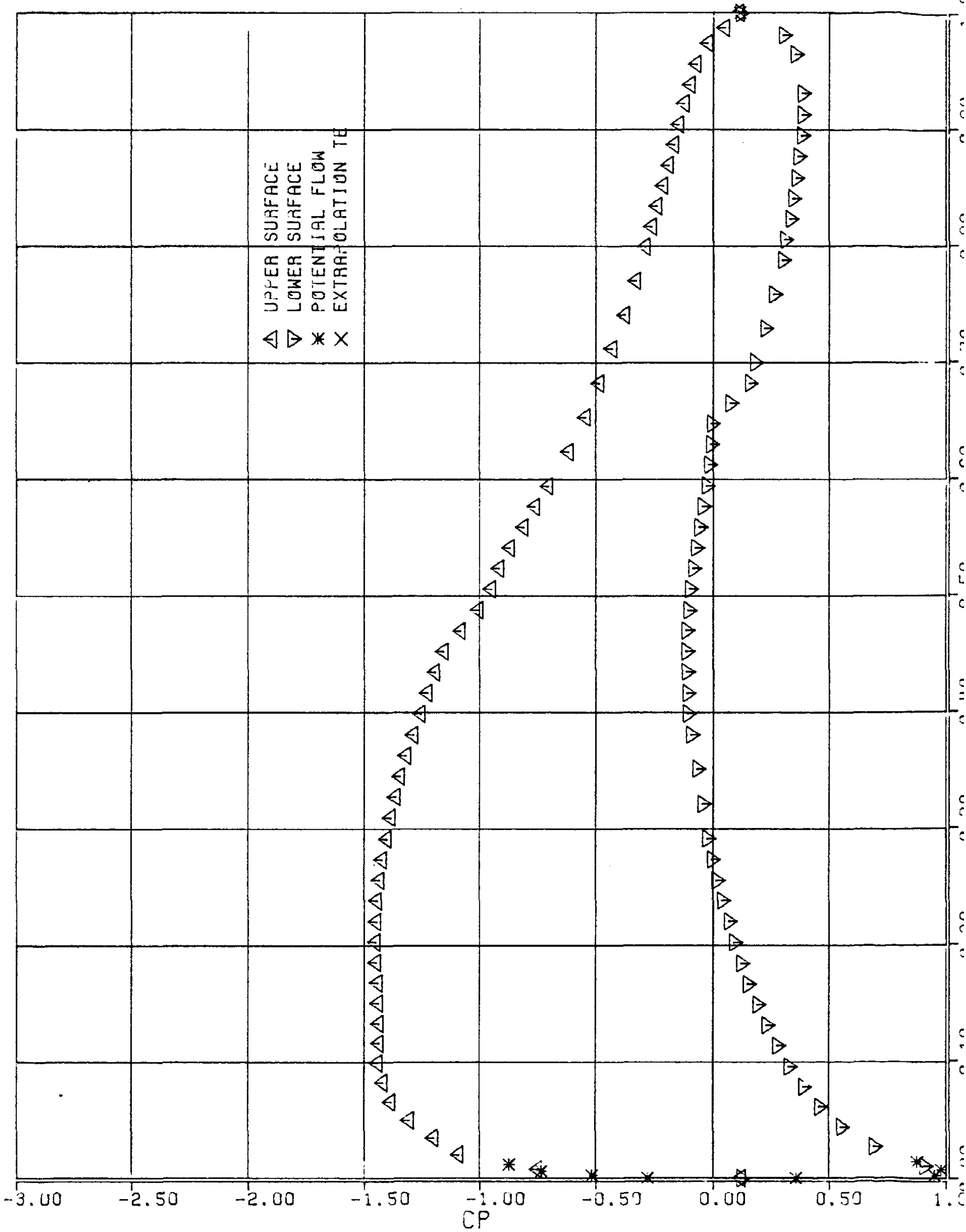

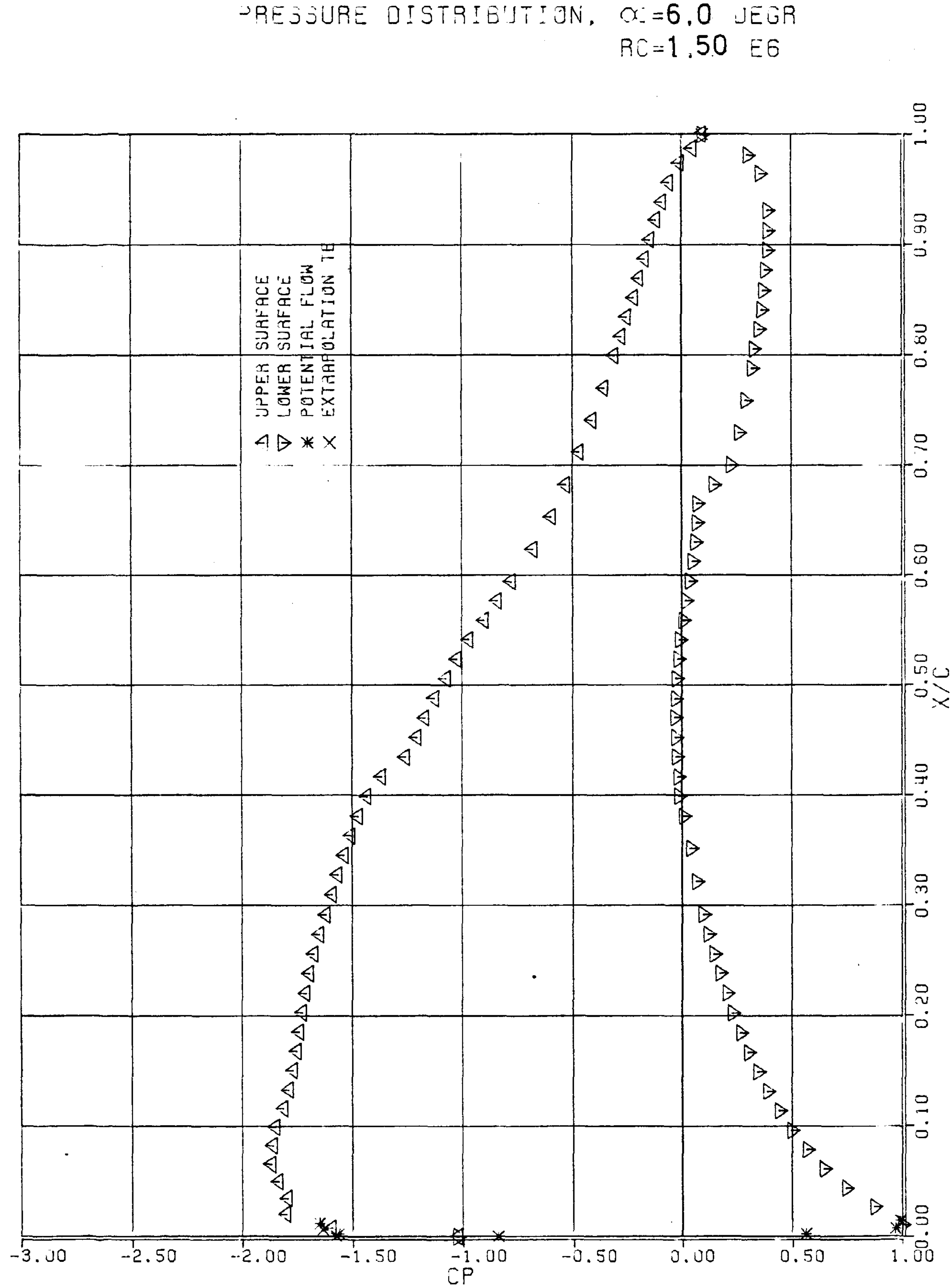

Figure 9.6 : Continued

PRESSURE DISTRIBUTION, α=8.0 DEGR
RC=1.50 E6

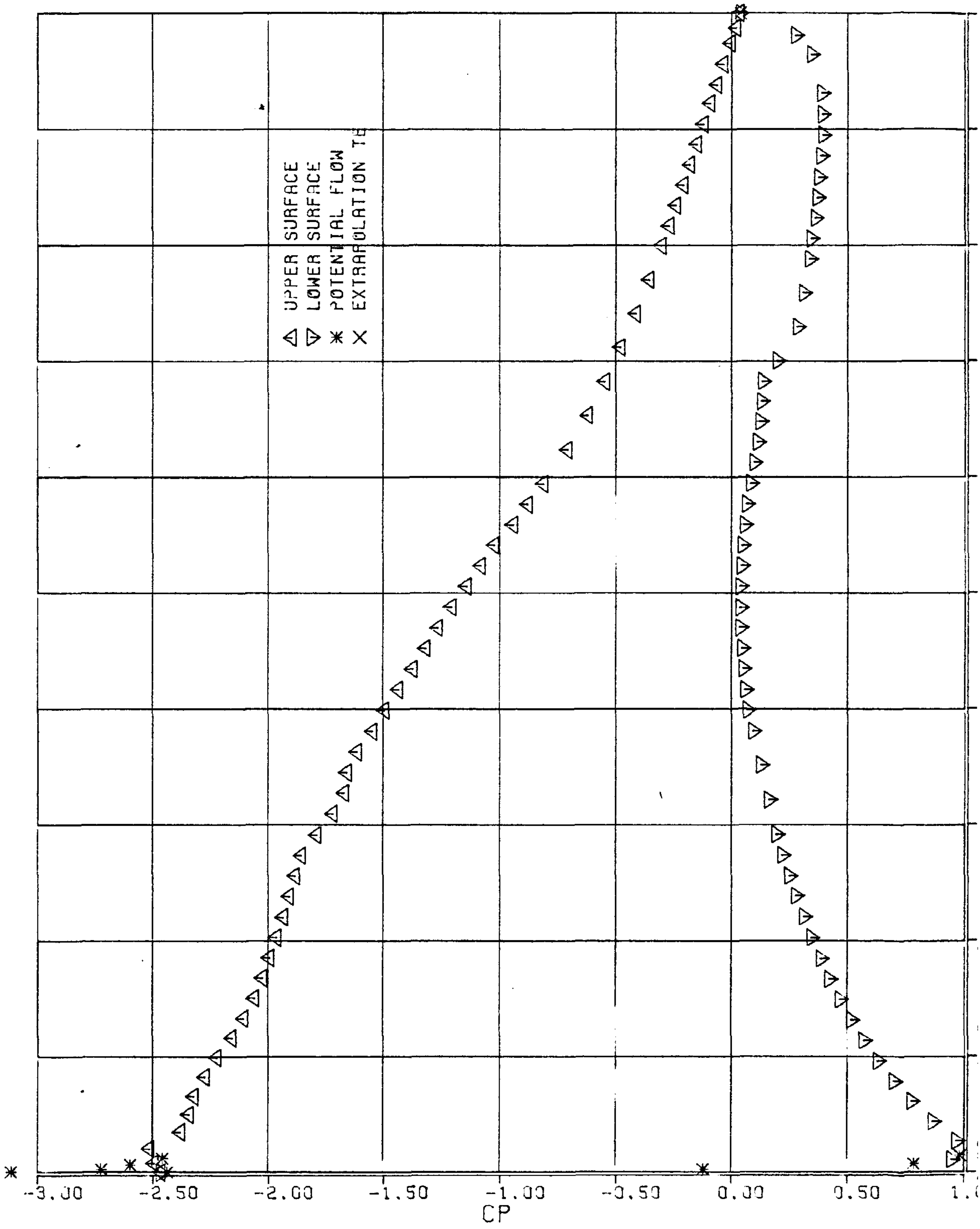

PRESSURE DISTRIBUTION, α = 10.0 DEGR
RC=1.50 E6

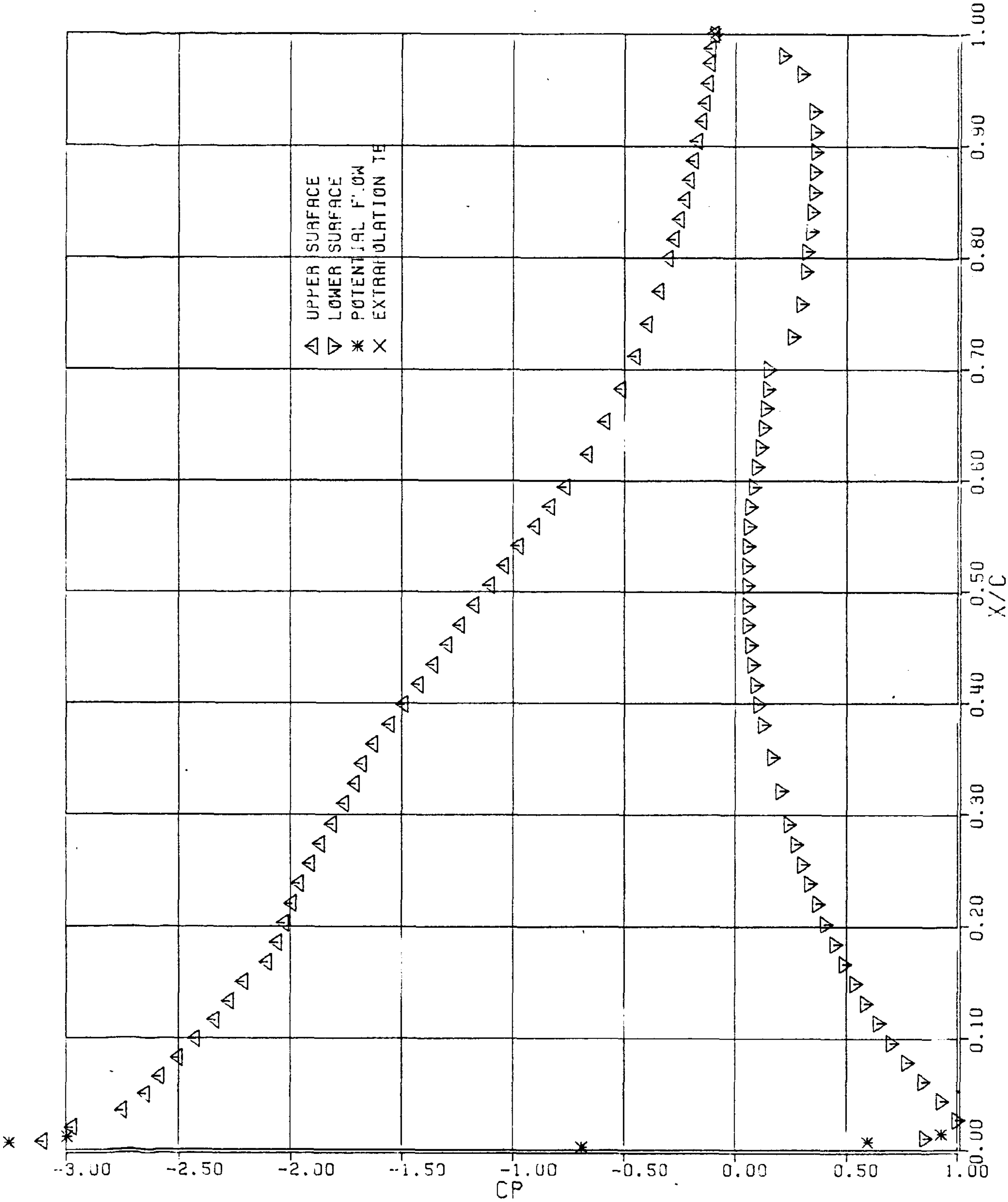

Figure 9.8 Continued

PRESSURE DISTRIBUTION, α=12.0 DEGR
RC=1.50 E6

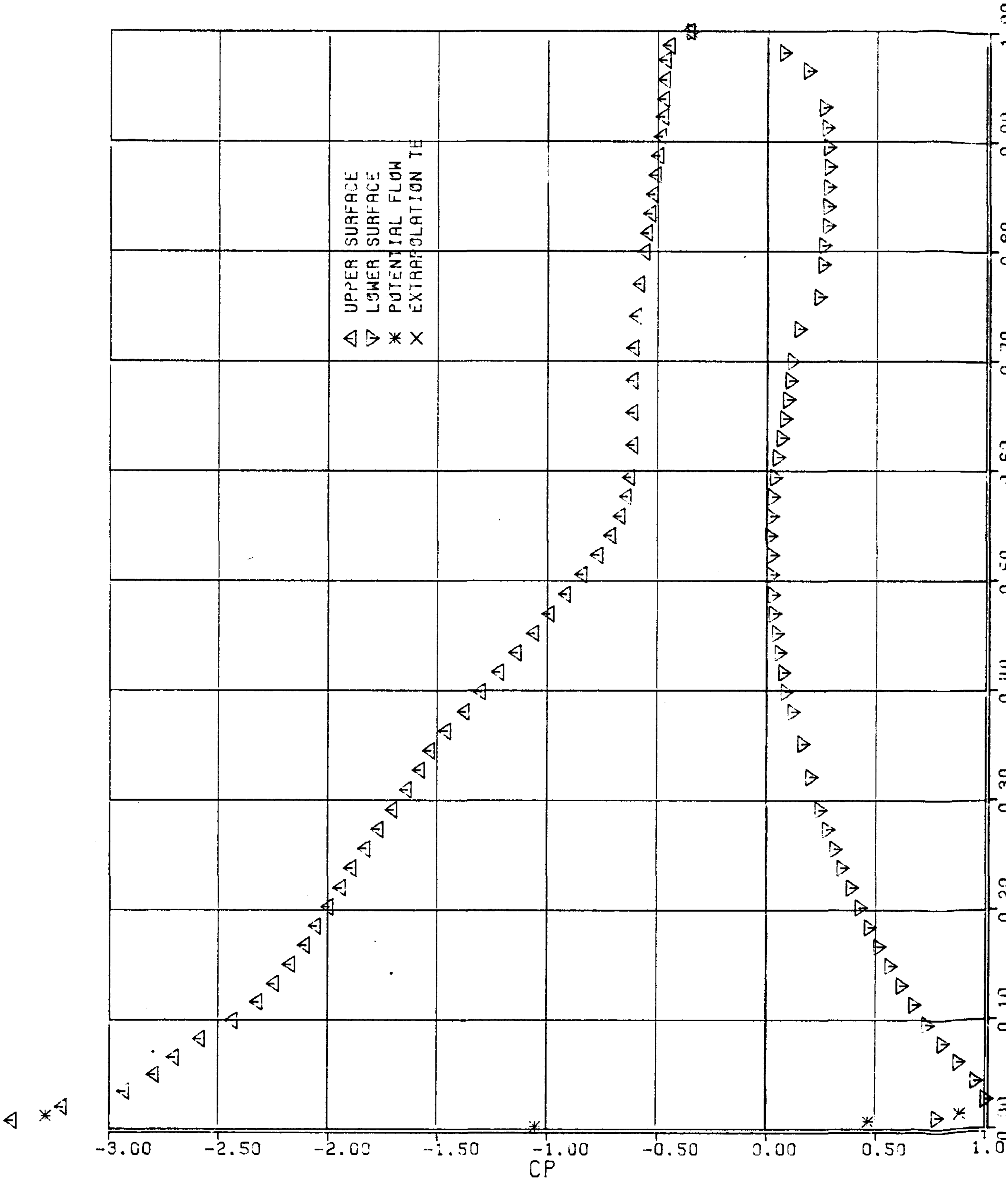

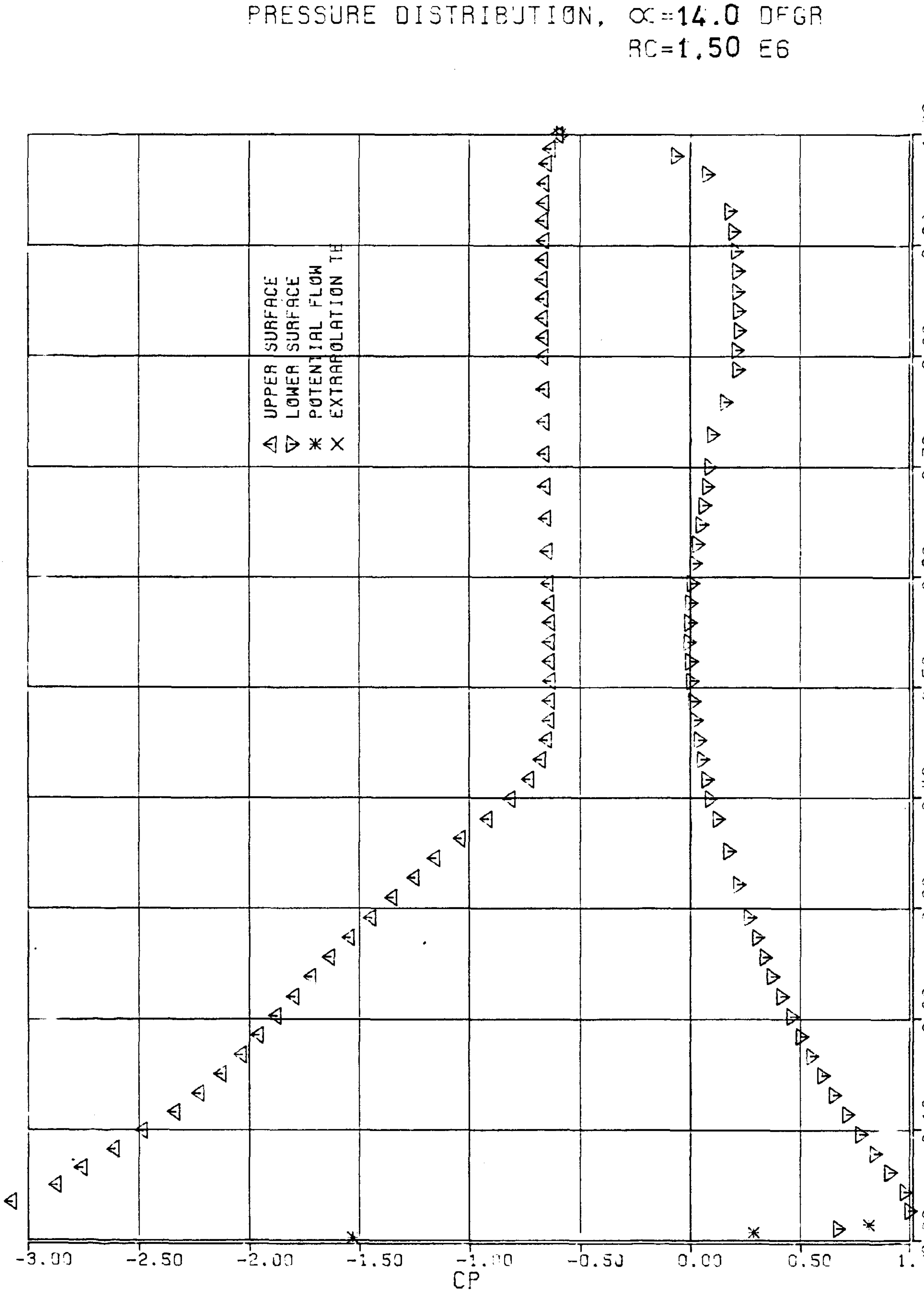

Figure 9.10 Continued

PRESSURE DISTRIBUTION, α=16.0 DEGR
RE=1.50 E6

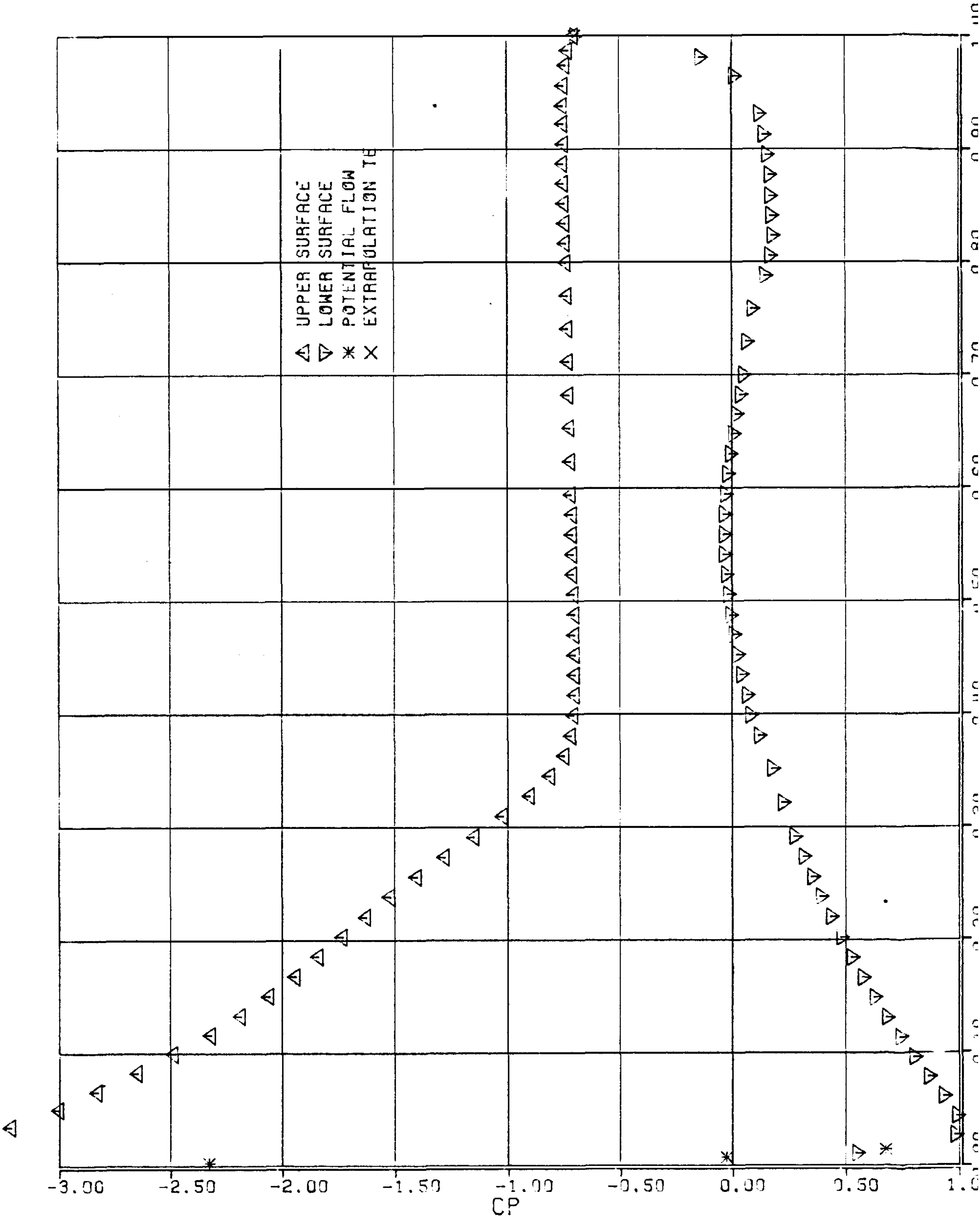

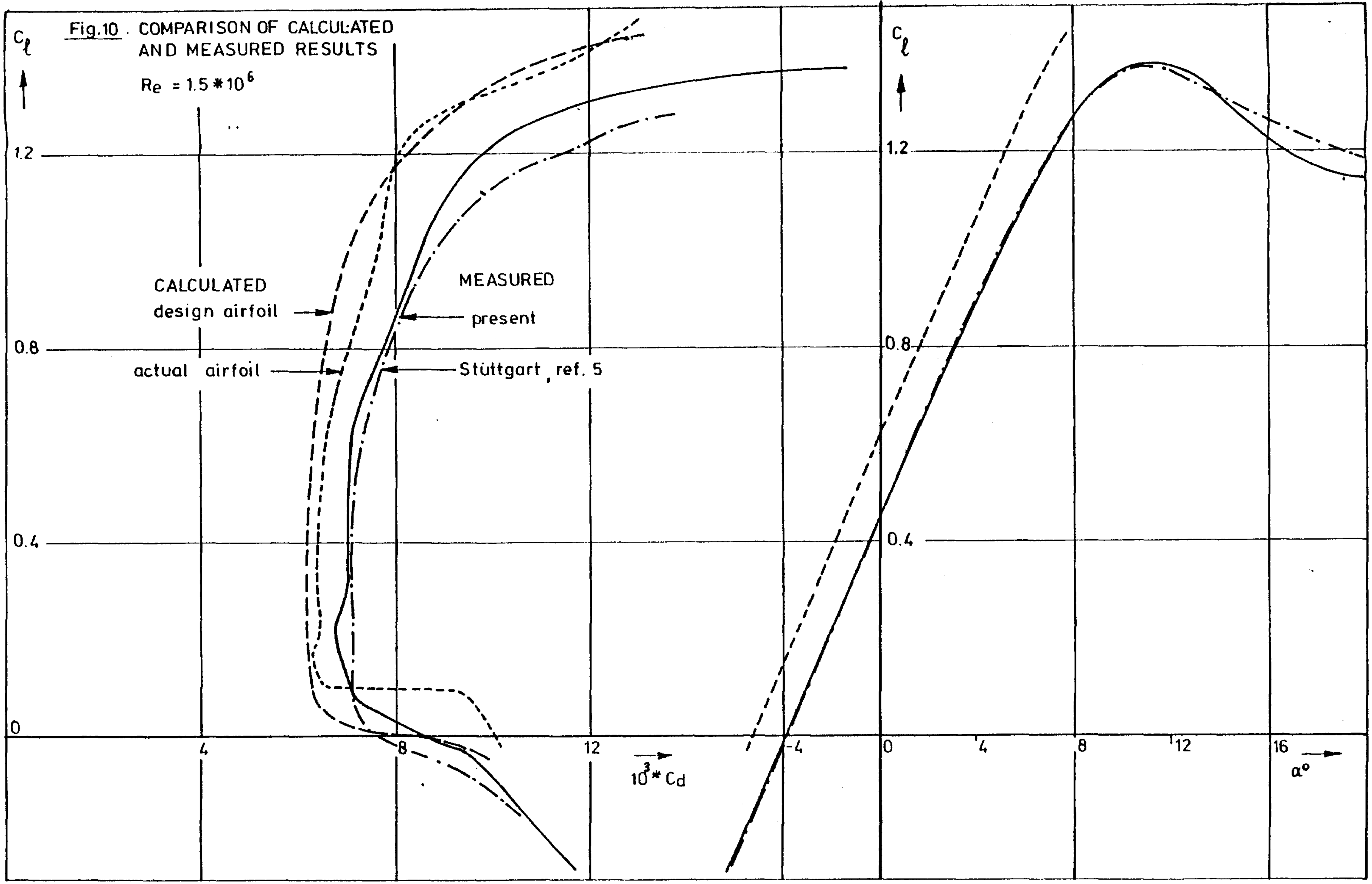

Fig.10 . COMPARISON OF CALCULATED AND MEASURED RESULTS

Fig. 11. Results of stethoscope investigation on model 2 mid span section.

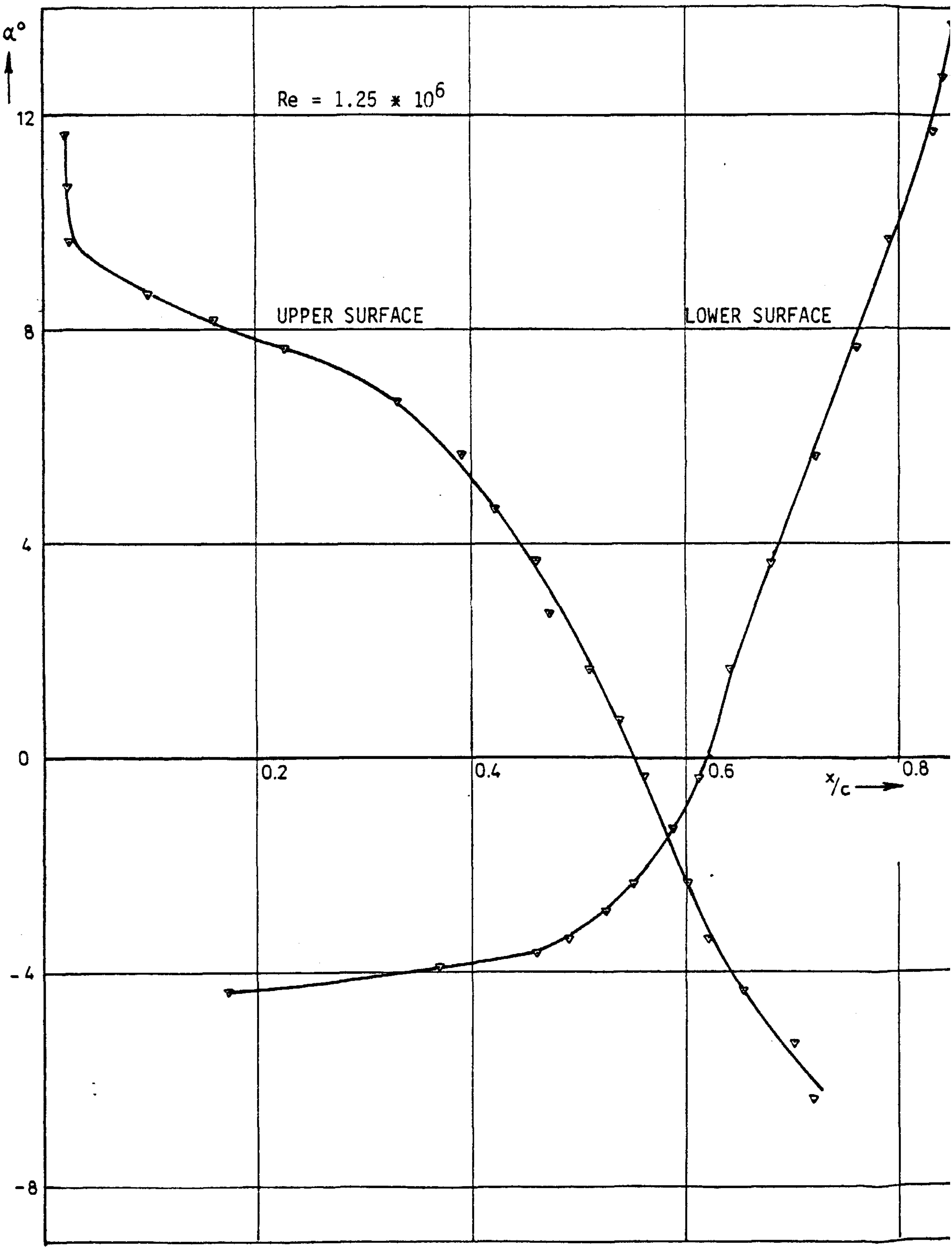

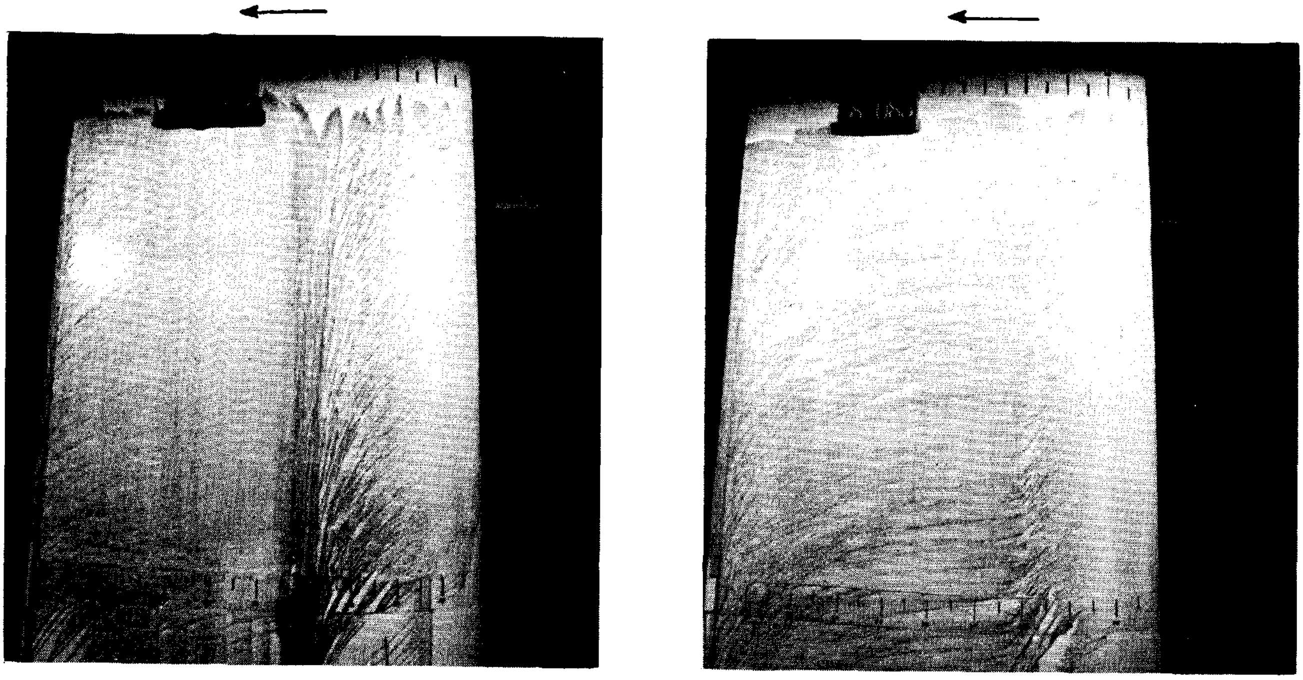

Upper surface
$\alpha = 5^{o}$
$Re = 0.85 * 10^{6}$

Upper surface
$\alpha = 8^{o}$
$Re = 0.85 * 10^{6}$

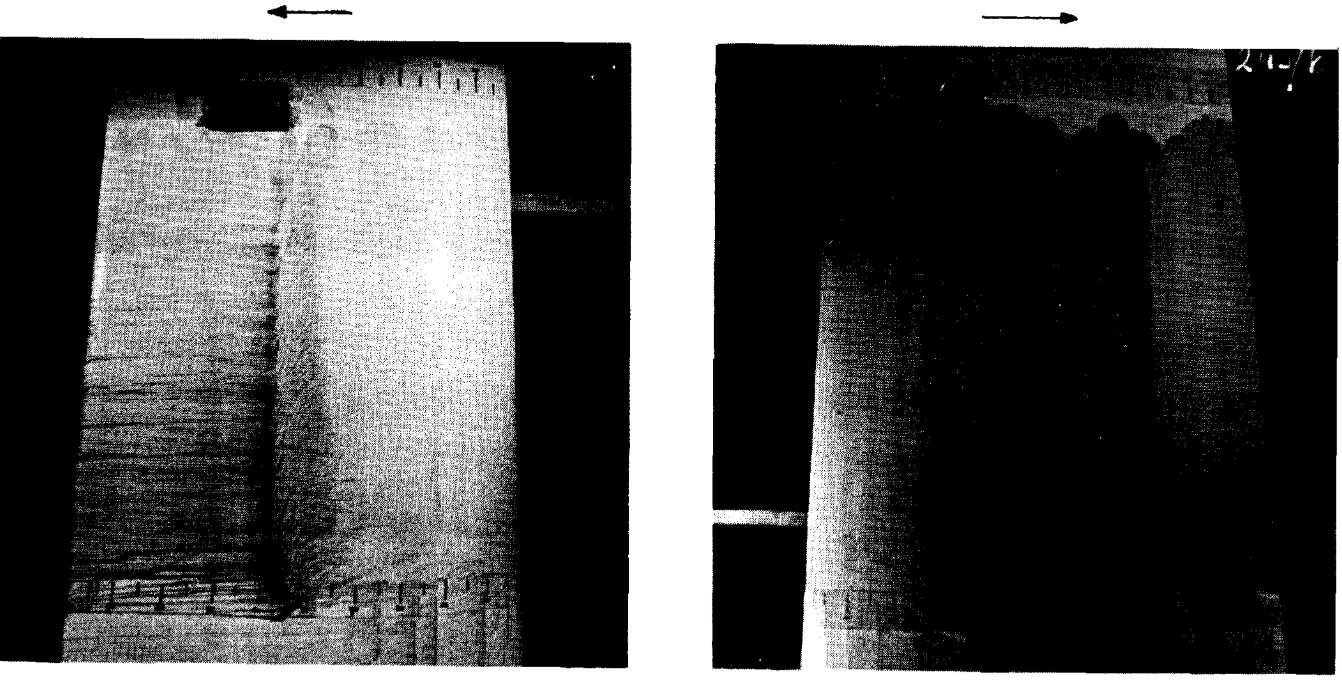

Upper surface
$\alpha = -2^{o}$
$Re = 2.0 * 10^{6}$

Lower surface
$\alpha = 8^{o}$
$Re = 0.85 * 10^{6}$

Fig. 12. Some oil-flow patterns of model 2.

Fig. 13. Comparison of section drag coefficients.

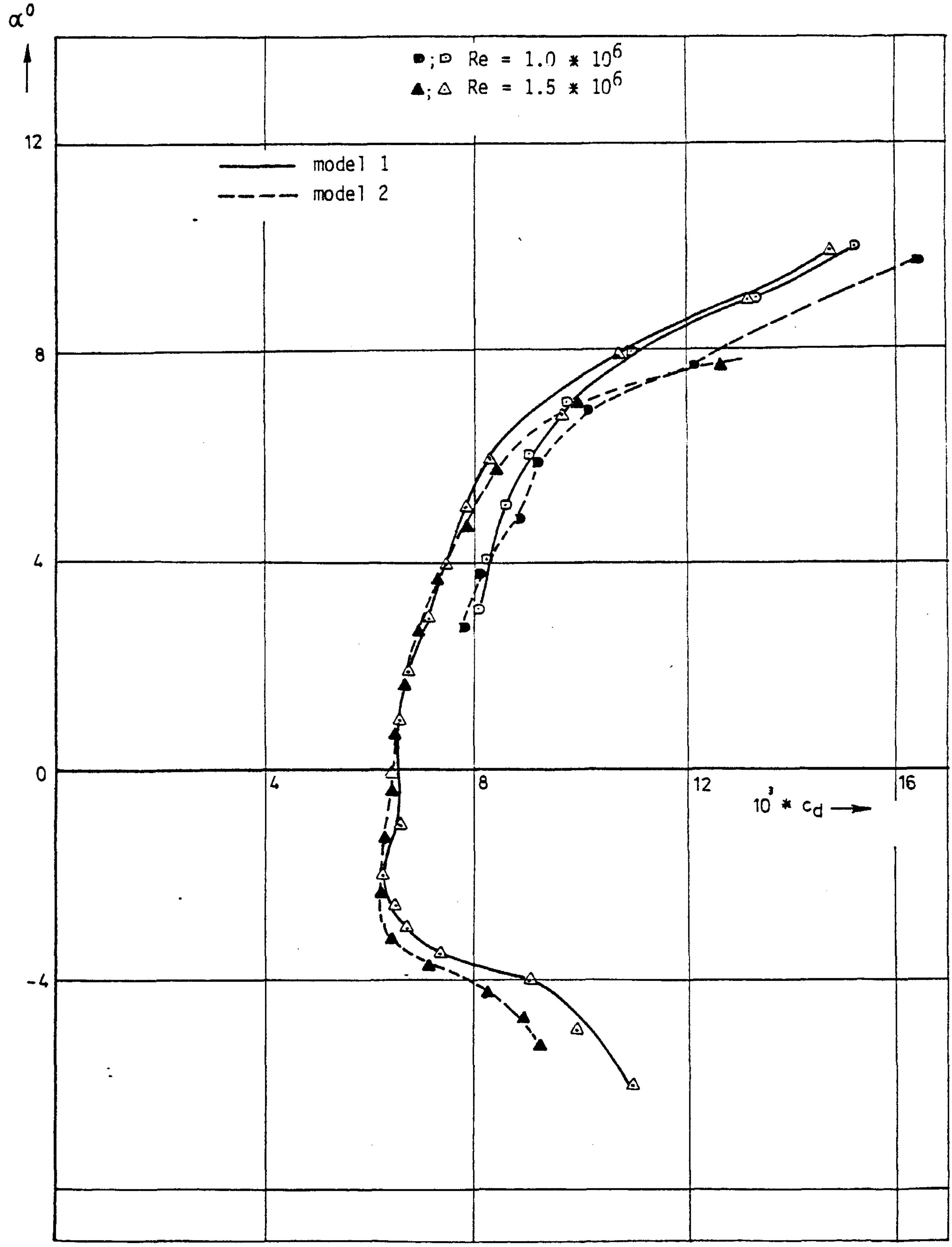

Fig. 14. Section characteristics.

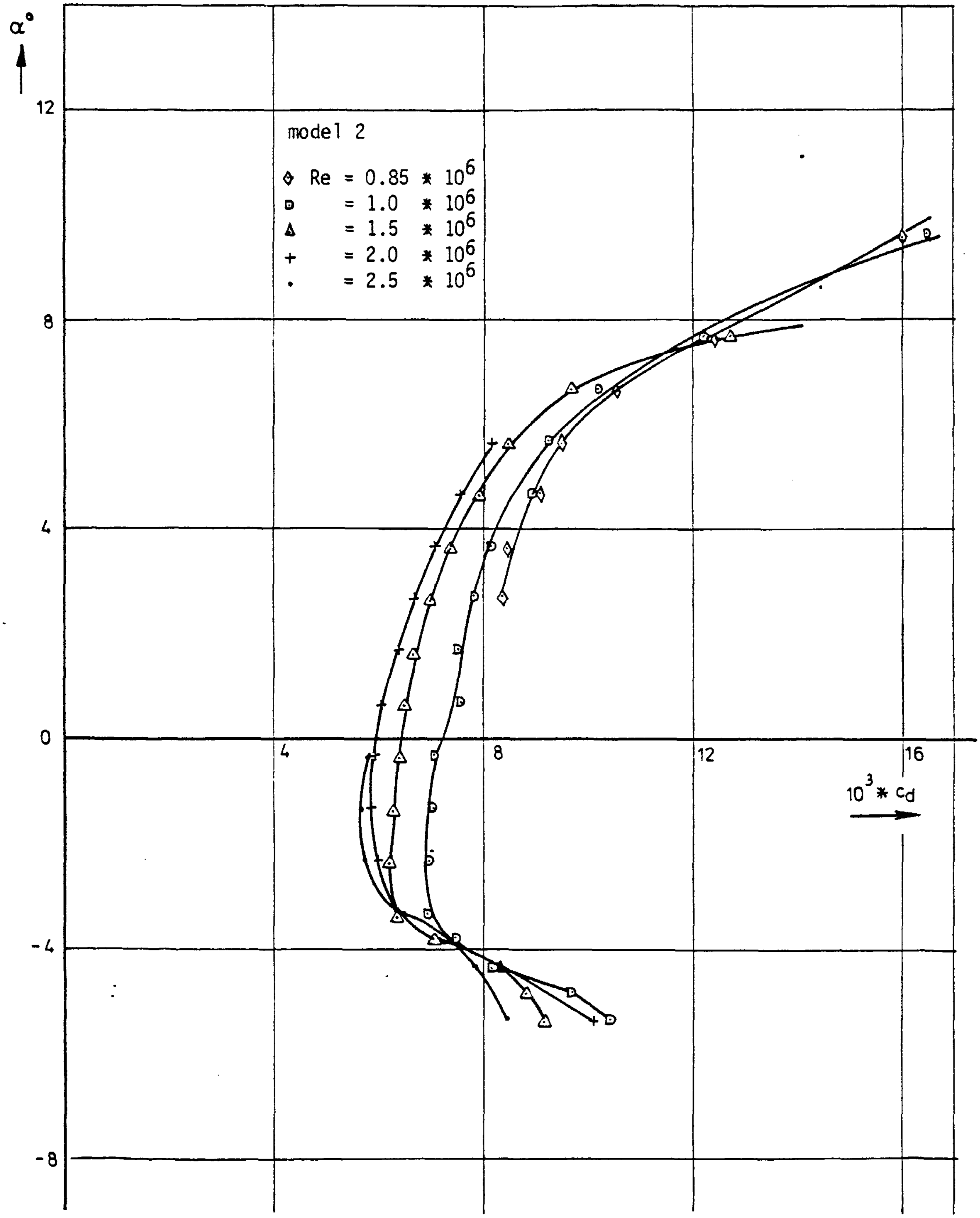

Fig. 15. Spanwise drag distribution for the buggy model 1.

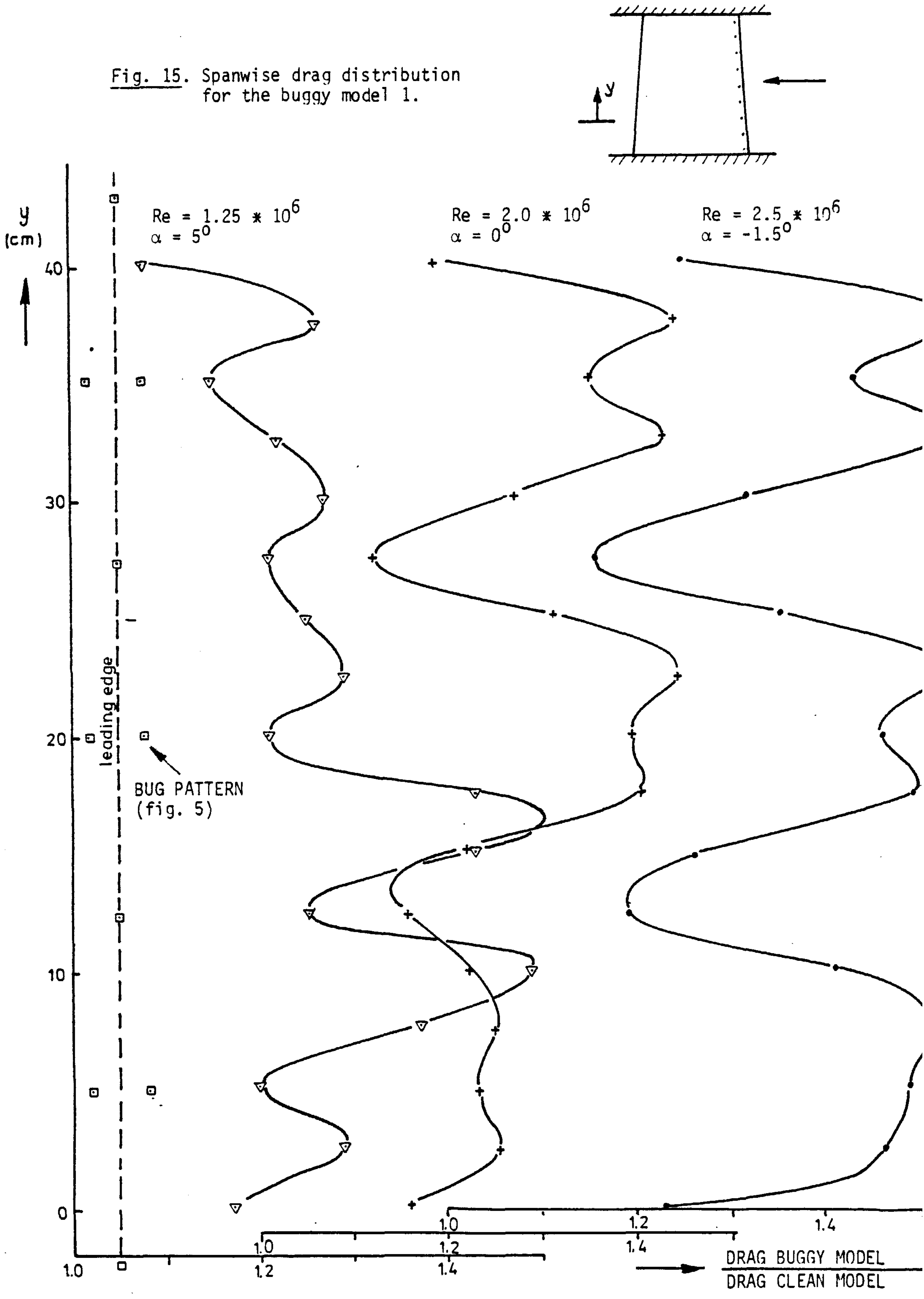

of model 1 with and without bugs.